Journal of the Ceramic Society of Japan 129 [6] 292-309 2021
DOI http://doi.org/10.2109/jcersj2.21004

JCS-Japan

FULL PAPER

Material combination conditions of the polymer infiltration and pyrolysis-melt infiltration hybrid process to make a dense and uniform matrix of SiC fiber-reinforced SiC matrix composite

Masaki KOTANI[1,†], Kohei EJIRI[2,‡], Takuma TANAKA[3], Takeshi TAKAGI[3], Takeo ODA[4], Takayuki KOJIMA[1] and Shinji OGIHARA[2]

[1] Aeronautical Technology Directorate, Japan Aerospace Exploration Agency (JAXA), 6–13–1 Osawa, Mitaka, Tokyo 181–0015, Japan
[2] Graduate School of Science and Technology, Tokyo University of Science, 2641 Yamazaki, Noda, Chiba 278–0022, Japan
[3] Corporate Technology Division, Kawasaki Heavy Industries, Ltd., 1–1 Kawasaki-cho, Akashi, Hyogo 673–8666, Japan
[4] Aerospace System Company, Kawasaki Heavy Industries, Ltd., 1–1 Kawasaki-cho, Akashi, Hyogo 673–8666, Japan

In this study we investigated methods of forming matrices of SiC/SiC composite, which have recently attracted considerable attention as high temperature structural materials that can be used in airplane engines etc. We examined ways of balancing the formation of the dense, strong microstructures with the infiltration into fibrous preforms. A process in which a green body was prepared by polymer infiltration and pyrolysis (PIP) processing, using slurry containing a liquid precursor polymer and fine powders, was densified using melt infiltration (MI) processing. Promising combinations of raw materials and their ratios were selected based on past research results. The microstructures and elemental distributions obtained from those materials after the last PIP processing and after the MI processing, as well as the thermal and mechanical properties of the composites, were comparatively evaluated. Thus, favorable conditions of raw material combinations to fabricate a high-performance matrix were determined.

Key-words : SiC/SiC composite, Polymer infiltration and pyrolysis, Melt infiltration, Microstructure, Thermal conductivity, Young's modulus

[Received January 4, 2021; Accepted March 23, 2021]

1. Introduction

With the growing demands for global air traffic and with a view toward the future, there is stronger demand than ever for the improvement of fuel efficiency of turbo-fan engines, aiming to reduce the cost of aircraft operations and to reduce the environmental burden due to CO_2 emissions. The increase of turbine inlet temperature is the most effective measure for the above. To this end, SiC fiber-reinforced SiC matrix (SiC/SiC) composites, which are lighter and more heat-resistant than conventionally used Ni-based heat-resistant alloys, are starting to be applied to the structural parts used at high temperatures, such as combustors and turbines.[1)]

There have been decades of research and development of SiC/SiC composites concerning their components, such as fibers, interface, and matrices, and promising candidates have been narrowed down for each component.[2)–4)] Based on the results, manufacturers and research institutions are currently hard at work on the selection of candidates, the pursuit of optimal conditions and technological development to reduce production time[5)–7)] in the aim of achieving properties suitable for applications and reduction of costs.

As for the forming of matrices, research on the forming of dense and uniform formative microstructures and their stable and highly efficient manufacturing has been pursued quite actively by sophisticating different conditions and effectively combining different technologies using the chemical vapor infiltration (CVI) method, the polymer infiltration and pyrolysis (PIP) method, and the melt infiltration (MI) method as basic techniques.[8)–10)] The CVI method is essential as a forming method of the interface and its outer layer as the only technique to form successive layers with high crystallographic purity and fewer defects, but it still requires a great deal of time, which leads to high cost, and the density that the whole material can achieve by this method alone is generally low. The PIP method has the advantage of being easier to start because of the availability of FRP manufacturing technologies and

† Corresponding author: M. Kotani; E-mail: kotani.masaki@jaxa.jp
‡ Present address: Kajima Corporation, 3–1 Motoakasaka 1-chome, Minato-ku, Tokyo 107–8388, Japan

facilities, but it requires a long period of time for repeated processing and it is difficult to obtain dense and strong ceramics microstructures with fewer cracks due to the precursor polymers. The MI method is currently the mainstream matrix formation method, with the advantage of being able to form relatively dense microstructures in a short period of time by using a material slurry mainly composed of fine powders. However, it confronts the challenges of uniform microstructure formation into fabrics and the restriction of heat-resistant temperature related to residual Si.

In light of the properties of the above methods, the method of forming the surface sliding layer (BN or C) and its outer layer (SiC) before or after weaving by the CVI method with sophisticated control, and to fill the remaining voids with the MI method has an advantage in many cases in terms of both material performance and costs. The prepreg layup method easily takes advantage of this characteristic, but filling the voids of fabric with fine powders is difficult when using the fiber fabric preform. It is largely impacted by the poor impregnation of the fine powder slurry and the formation of voids after the evaporation of liquid components, such as solvent in the slurry.

A Japanese study once reported a result on the acquisition of a strong monolithic material with a high SiC yield by highly controlling the uniform and fine distribution and volume fractions of SiC and C fine powders that composed the green matrix of the MI processing and the voids among the fine powders.[11] But the following study report showed that it was difficult for fine powder materials on their own to form dense matrices in the voids of fiber fabrics for composites.[12]

On the other hand, replacing part of the fine powder materials with liquid precursor polymer can improve the impregnating ability of slurry and reduce or eliminate the solvent. While this process may be called the PIP method as it uses precursor polymers, a large number of processes that combine the PIP method and the MI method have been tried so far as reasonable approaches utilizing their respective characteristics.[13),14] In this regard, however, it is difficult to control microstructures with the PIP method, and there has been the need to form a green matrix suitable for the MI method by cleverly controlling the microstructures and to acquire dense and strong microstructures with high SiC yield (less unreacted C and residual Si). So far, there has been no study report that significantly realizes the above and provides clear guidelines.

In this study, we investigated the combination and the blending ratios of the raw materials to obtain a dense and uniform matrix of SiC/SiC composite with a process combining the PIP and MI methods, in reference to the MI conditions of the above-mentioned Reference literature 11. We addressed a set of combinations of liquid precursor polymer and fine powders, and set the blending ratios with which we can have expectations for the compatibility of the impregnating ability and the formation of dense and strong microstructures. Section 2.2 “Conditions settings for matrix raw materials” explains the selection thereof in detail. By investigating the three PIP raw material conditions, the microstructures after the last PIP processing (before the MI processing), and the microstructures after the MI processing in correlation, we judged the adequacy of the raw material conditions. In this report, we dealt with the microstructures formed in the voids in the fibers from raw materials, and will report on the impregnating ability/impregnating method with regard to the reinforced fiber fabrics of raw materials.

2. Experiment methods

2.1 Preparation procedures of samples of composites

Samples of composites were prepared according to the procedures shown in **Fig. 1**. A Tyranno fiber SA 8-harness satin woven sheet (Ube Industries, Ltd., Japan) cut to the size of 40 mm × 40 mm, was used as the reinforcing material. No interface layer forming processing was conducted.

Raw material slurries for the matrices under the respective conditions were evenly impregnated on the samples in as constant an amount as possible. Twelve sheets with slurry impregnated were laminated in the formation mold, which was heated up to 1000 °C in an argon atmosphere with uniaxial pressing in a resistance heating furnace (Fuji Dempa Kogyo Co., Ltd., Japan). We call this process “press forming.” We impregnated the same slurry as used in the press forming in vacuum, and fired the samples under the same conditions as those of press forming without pressurizing them. After repeating this vacuum impregnation/firing process the same number of times as for the samples of all the raw material combinations, we obtained a PIP-derived green matrix composite of 40 mm × 40 mm × 3–5 mm of outer dimensions. We put them into Si raw materials in a graphite vessel, and heated them to 1450 °C under reduced pressure in the same furnace. The obtained PIP-MI composites were defined as the final samples, and were used for different evaluations.

In addition to the above samples, we also prepared samples of uni-directionally reinforced composite with outer dimensions of 150 mm × 15 mm × 4–6 mm for impulse excitation tests for the combinations of all the raw

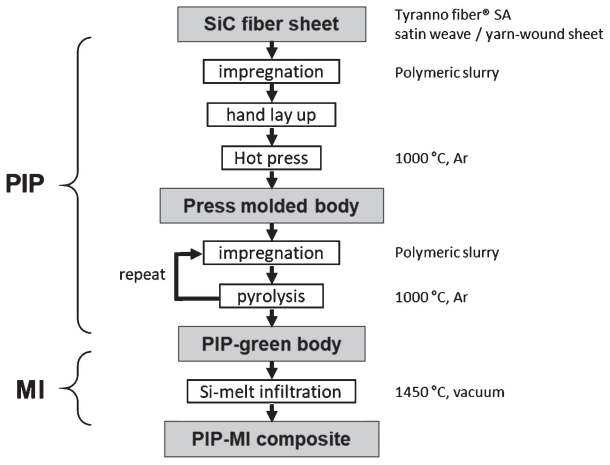

Fig. 1. Fabrication procedure of composite samples.

materials. A uni-directional sheet prepared by winding Tyranno fiber SA bundles (800 filaments/bundle) was used as the reinforced material, and all other preparation conditions were the same as above.

The unevenness of the sample thickness was caused by the difference in the amount of slurry from the laminated sheets due to pressurizing in the press-forming. It seems that blending ratios of the solid component (powder) that determines the fluidity of the slurry have had a great impact. The fiber volume fractions (V_f) of the ultimately obtained samples vary depending on the impact. The weight per sheet unit area was obtained for the satin woven sheet laminated materials, and the weight per unit length of fiber bundle was obtained for the winding sheet laminated material by measurement, respectively. The total fiber volumes contained in the respective samples were calculated from the above measurements and the fiber density value ($3.1\,g/cm^{-3}$) presented as the inspection results by the fiber manufacturer to obtain V_f, and the results were scattered in the range of 25 to 50 %. As the above results were peculiar to the press forming, we excluded the impact caused by the difference of V_f as much as possible for the discussion, by focusing on the matrix formed in the voids of reinforced material from the raw materials.

2.2 Condition settings for matrix raw materials

In addition to the SiC raw material-in-liquid series and the C raw material-in-liquid series, we also added an all-SiC raw material series without C raw material as one of the combinations of SiC and C raw materials. The aim of the third series was to conduct relative evaluation of the effectiveness of the approach that would reinforce the residual voids after the formation of an all-SiC matrix framework by the ordinary PIP method by filling with Si, even if only slightly. In other words, as the combinations of PIP raw materials to make the green matrix for MI in this study, we set three series: <Liquid SiC precursor polymer + C powder>, <Liquid C precursor polymer + SiC powder> and <Liquid SiC precursor polymer + SiC powder>. In the following, the combination of raw materials such as Composition A and Composition B is stated as <A + B>. Furthermore, we established the combinations to blend pore-forming powder that disappeared by thermal decomposition during baking and formed micropores there, aiming at the uniform distribution of PIP formation microstructures and the expansion of the specific surface area that increases the occasions of reaction with molten Si in the MI processing for each of the three series.

Figure 2 summarizes the combinations of six kinds of raw materials in total. As the basic PIP type that did not include C raw materials, we listed the types starting with <Liquid SiC precursor polymer + SiC powder>. After that, the IDs of #1 to #6 shown herein were used as appropriate for the respective combinations. We properly evaluated the relative merits as the MI green matrix raw materials among these combinations, and further extracted

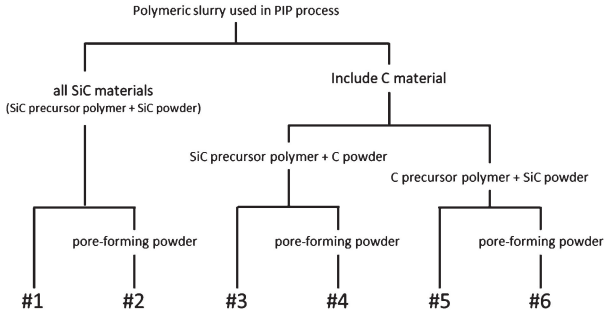

Fig. 2. Raw material combinations used to make PIP-derived green matrices for MI processing.

the guidelines for blending conditions to obtain better microstructures among the respective combinations.

As raw materials, we used liquid polycarbosilane of approximately 70 wt % of yield for the SiC precursor polymer; liquid phenol resin of approximately 30 wt % of yield for the C precursor polymer; pulverized powder of no greater than 1 μm of average particle size for the SiC powder; carbon black of no greater than 0.1 μm of particle size for the C powder; and polymethyl methacrylate powder with no greater than 5 μm of particle size for the pore-forming powder. As solvents for these, we used hexane for the SiC precursor polymer and ethanol for the C precursor polymer, as appropriate. The hardening of both kinds of precursor polymer above was almost complete before 200 °C was reached, and the pore-forming powder started to disappear due to thermal decomposition from around 200 °C to form pores.

We established standard blending conditions for each combination of raw materials from the results of the former research listed below (i) to (iii) and the results of qualitative consideration of the ability to impregnate fiber fabrics. We established the basic guideline that we should obtain green matrix microstructures that are as close to (iii) as possible from the slurry of the powder blending ratio in consideration of (i), and established the highest blending ratio we could base on (ii) while considering (i) when applying the pore-forming powder.

(i) When forming matrices in the fiber voids from the slurry added with powder to the liquid precursor polymer, from the viewpoints of its fluidity and the volumetric yield after thermal decomposition, relatively uniform and dense microstructures were obtained at approximately 30–50 wt % (≈ 15–25 vol %) (inner percentage) of the powder blending ratio.[15)]

(ii) When obtaining a porous body formed by thermal decomposition from the slurry added with pore-forming powder to liquid precursor polymer, from the viewpoint of the stability of microstructures during thermal decomposing shrinkage, porous microstructures with relatively fewer cracks were obtained at approximately 65 vol % (≈ 70 wt %) (inner percentage) of the pore-forming powder blending ratio.[16)]

(iii) The volume fractions of SiC, C, and pores in the green matrix before the MI processing from which

SiC microstructures with fewer gas pockets, cracks, and residual Si can be obtained after MI processing were approximately 35 vol %, 30 vol %, and 35 vol % (inner percentage), respectively.[11)]

In the experiment, we controlled the raw materials at an easily controllable weight and set the blending ratios of raw material combinations #1 to #6 as shown in i) to iv) below:

i) The weight ratio of SiC powder was unified to that of the precursor polymer. (#1, #5, and #6)
ii) For the C powder whose particle size was smaller than that of the SiC powder and that might increase the viscosity of the slurry, the weight ratio to the precursor polymer was set slightly lower (#3 and #4).
iii) The weight ratios of the pore-forming powder to the sum of the precursor polymer and the powder were unified for #4 and #6. For #2, the weight ratio was set higher, giving greater importance to (ii) above.
iv) We determined that the fluidity of the slurry should be improved for the combinations other than #1, and we added solvents. The weight ratios of addition to all the blending raw materials were unified for #2, #4, #5, and #6. The fraction was set slightly lower for #3, which showed relatively higher fluidity.

We explain the slurries for #1 to #6 set as above from the aspect of the volume fraction of the constituent raw materials as a factor mainly related to the viscosity/fluidity. **Figures 3**(a) and 3(b) show the volume fractions of raw materials in all the components of the combinations of raw materials, including and excluding the solvents, respectively. In all the components including the solvents, the volume fraction of SiC powder or C powder was approximately 10 vol % and that of the pore-forming powder was approximately 15 vol %, while that of the pore-forming powder for #2 was 30-odd vol %. In the components excluding the solvents, the volume fraction of SiC powder or C powder was 10-odd vol %; and in the series that introduced pore-forming powder other than #2, the pore-forming powder included approximately 20 vol %, which made all the contained solid components to 30-odd vol %. In #2, the contained solid components were more than 40 vol %. We will report on the quantification of the viscous property of the above in another report concerning the impregnation of slurry.

As the factor directly related to the efficiency of densification as the PIP raw materials of slurry, **Figs. 4**(a) and 4(b) show the volumetric yields of the products obtained after thermal decomposition from all the components including the solvents and excluding the solvents, respectively. We calculated the volumetric yields, assuming that the pore-forming powders had disappeared and that the volume of SiC powders and C powders was unchanged. As the disappeared pore-forming powders formed micropores at the positions where they existed, its impact on the microstructure formation was different from that of the thermal decomposing shrinkage of precursor polymer. The impact of the pore-forming powders is

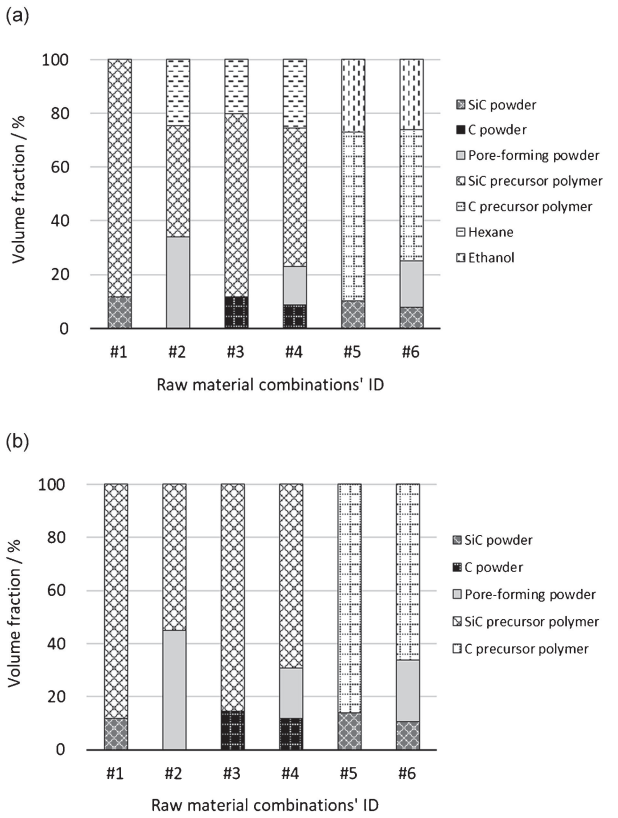

Fig. 3. Volume fractions of the constituent raw materials of the slurries. Solvent is present and absent in (a) and (b), respectively.

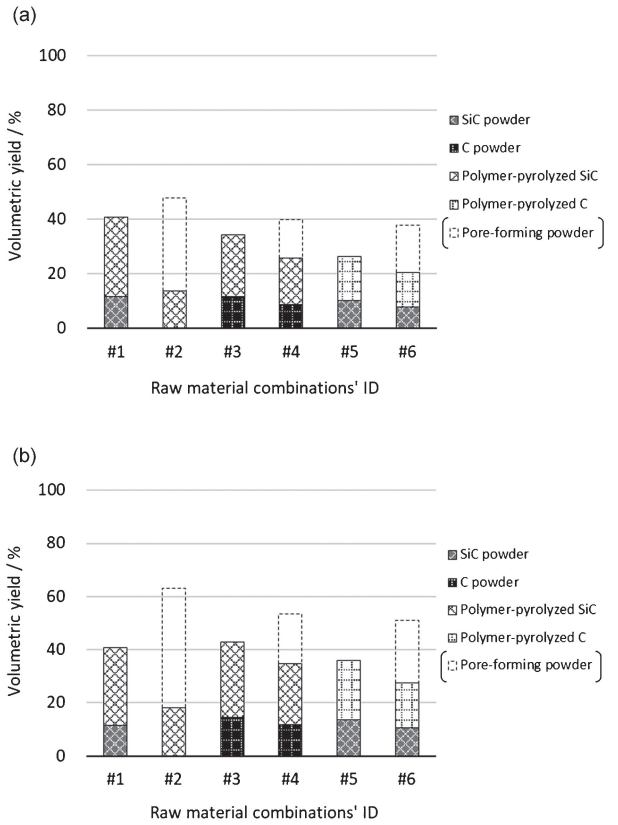

Fig. 4. Volumetric yields of the slurries after the heat treatment. Solvent is present and absent in (a) and (b), respectively.

shown with dotted lines in said figure. The yields from all the components in Fig. 4(a) correspond to the volumetric residual ratio of the products remaining after thermal processing from the raw materials that existed in the voids among fibers when the slurry was formed together with the fiber materials, or when the slurry was impregnated into fiber preforms; the yields from the components excluding the solvents of Fig. 4(b) correspond to the volumetric residual ratios of the products remaining after the thermal processing from the raw materials that existed in the voids of fibers when they were further dried. The volumetric yields of #1 and #3 were relatively higher, showing that these combinations have an advantage in terms of densification. Comparing the combination of the same materials, as a result of the consideration of the fluidity of the slurry, the combinations blended with pore-forming powder (#2, #4, and #6) showed lower volumetric yields than the combinations without blending pore-forming powder (#1, #3, and #5). If the voids minutely dispersed in the products by the pore-forming powder are deemed to be part of the products, their relationship reverses.

Figures 5(a) and 5(b) show the volume fractions of the components derived from raw materials in the thermally decomposed products of these slurries as the main factor of microstructure formation in MI processing. The volume fractions in Fig. 5(a) were calculated by using the values obtained with pycnometry for the density of thermally decomposed products of the precursor polymers, and these showed the volumetric content in the actual samples. On the other hand, the volume fractions in Fig. 5(b) were calculated by using the literature data of SiC and C of highly pure crystals for the density of thermally decomposed products of precursor polymers. In the Reference literature 11, the above results of preceding study (iii) were obtained by using highly crystalline SiC and C powders. If the results were mainly influenced by the physical volume fractions of the respective components in the MI green matrix, the information in Fig. 5(a) should be noted. On the contrary, if the results were mainly influenced by the ratio of the quantity of substances (the number of atoms), the information in Fig. 5(b) should be noted. Said document states that it is desirable that the SiC, C, and voids in the MI green matrix should have almost the same volume fractions of one third, in other words, that SiC and C should have close volumetric ratios. If supporting Fig. 5(b), the amounts of substances of SiC and C for #3 to #6 were each close to half, which seems to be a proper condition to a certain extent in this point. The voids of the remaining components were formed by the shrinkage of gas bubbles and the volume contraction due to the thermal decomposition of the precursor polymer and the disappearance of pore-forming powder. Each combination of raw materials attracts attention with the closeness of the formed microstructures to the results realized in Reference literature 11.

2.3 Evaluations of samples of composites

Relative comparative evaluation was conducted on the material microstructure, thermal characteristics, and

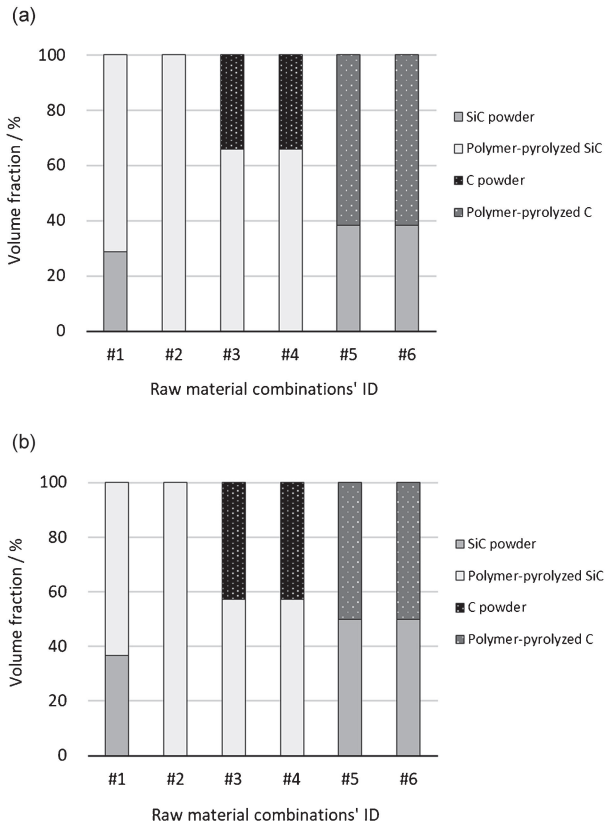

Fig. 5. Volume fractions of the constituents of slurry-pyrolyzed products. The densities of the pyrolyzed SiC and C from, (a) measured values by pycnometry, and (b) literature information for crystalline materials, were used in calculation.

mechanical characteristics of composites obtained from the combinations of raw materials. For the material microstructures, in order to evaluate the matrix densification trends and formed microstructures in the PIP processing process, the microstructures previously provided to the MI processing through the last PIP processing, and the microstructures after the MI processing, we conducted micropore distribution measurement using a mercury intrusion porosimetry test, observation of microstructures with an optical microscope, and element distribution analysis with an electronic probe micro-analyzer (EPMA) on the samples that went through the respective processes.

The mercury intrusion porosimetry test was conducted in accordance with the test standard JIS R 1655:2003 on the test samples with the dimensions of 15 mm × 14 mm × 2 mm cut out from the production samples using a micropore distribution measuring apparatus, Auto Pore IV 9505, a product of Micromeritics Instrument Corporation. In the measurement, a distribution of volume fractions of open pores with diameters of 0.01 to 400 μm in the samples was obtained. Microstructure observation was conducted on a cross section of the cut-out specimens of production samples embedded in the epoxy resin and polished, by using a metallurgical microscope, ECLIPSE MA200, a product of NIKON CORPORATION, and a microscope, VHX-5000, a product of KEYENCE CORPORATION. Element distribution analysis was conducted on a cross section of the

same samples using an EPMA JXA-8100, a product of JEOL Ltd.

As for the thermal characteristics, the heat conductivity in the outer direction of the reinforced fiber sheet lamination plane was measured in accordance with test standard JIS R 1611:2010 from the ambient temperature to 1200 °C at an interval of 200 °C. Discoid test specimens of 10 mm (diameter) × 2–3 mm (thickness) and rectangular solid test specimens of 3.5 mm × 3.5 mm × 1.3 mm were cut out from the composite sample after the MI processing, and provided to the measurement of the thermal diffusivity and specific heat necessary for the calculation of heat conductivity respectively. The thermal diffusivity was measured from the ambient temperature to 1200 °C at an interval of 200 °C in a vacuum, using a thermal constant measuring instrument, LFA-502, a product of KYOTO ELECTRONICS MANUFACTURING CO., LTD., with the laser flash method. The specific heat was measured with differential scanning calorimetry (DSC) in an argon atmosphere. DSC 3500 Sirius, a product of NETZSCH GmbH, was used to measure at the ambient temperature, and DSC 404 F1 Pegasus, a product of the same company, was used for other measurements up to 1200 °C. The density was calculated from the measurement of dimensions and the mass of test samples for thermal diffusivity measurement in the ambient temperature, and the measurement was applied to all the temperatures. The thermal conductivity λ was calculated based on Formula (1) from the thermal diffusivity a, specific heat C_p, and density ρ of respective temperatures.

$$\lambda_c = a \cdot C_p \cdot \rho \tag{1}$$

From the obtained thermal conductivity λ_c of all the composite samples, the estimated value of thermal conductivity λ_m for only the matrix part was calculated using the V_f of the respective samples and the thermal conductivity λ_f of the fibers, based on Formula (2) led from the compound rule of the series model.

$$\frac{1}{\lambda_c} = (1 - V_f)\frac{1}{\lambda_m} + \frac{V_f}{\lambda_f} \tag{2}$$

Concerning λ_f, only the values for ambient temperature (65 $W \cdot m^{-1} \cdot K^{-1}$)[17] are published from the manufacturer of the fiber. For the values for other temperatures, in reference to the data on multi-crystal SiC in Network Database System for Thermophysical Property Data,[18] available on the National Institute of Advanced Industrial Science and Technology website, we used the assumed values corresponding to the exponential function that decreases with the increase of the temperature and shows 30 $W \cdot m^{-1} \cdot K^{-1}$ at 1200 °C.

With regard to the mechanical properties, we measured Young's modulus in the one-way reinforcing direction from the ambient temperature to 1400 °C with the resonance method. We prepared strip-shaped test specimens of 60 mm × 10 mm × 2 mm cut out from the samples after MI processing to ensure that the fiber direction is in the longitudinal direction, measured the bending resonant frequency f_f in excitation by tapping the center of the test specimens in an argon atmosphere at various temperatures by using the resonant frequency/attenuation analyzer RFDA HT1600, a product of IMCE NV, and calculated Young's modulus E_c in accordance with Formula (3), in which "m" means the mass of the test specimen, "L" the length, "w" the width, "t" the thickness, and "T" the correction term. T is a value determined from the data of a standard sample whose elastic modulus is known. The impact of the thermal expansion of the sample was neglected, according to the estimation that the error on the elastic modulus may be approximately 0.5 % at the largest.

$$E_c = 0.9465\left(\frac{m \cdot {f_f}^2}{w}\right)\left(\frac{L^3}{t^3}\right)T \tag{3}$$

We tried to estimate the Young's modulus E_m of the matrix part only from the measurement results of all the obtained composite samples based on the compound rule of the parallel model $E_c = E_f V_f + E_m(1 - V_f)$. Concerning the value of E_f thereof, there is the value of inspection results from the manufacturer (377 GPa) as well as the published value close thereto (380 GPa).[17] We also discussed this point.

3. Test results and discussions

3.1 Comparison of density/pore distribution among the combinations of raw materials

Figure 6 shows the open porosity of only the matrices in the samples after the last PIP processing and MI processing obtained using the mercury intrusion porosimetry test of the respective combinations of raw materials. The above open porosity was obtained by dividing the open porosity obtained in the test of all the samples by the volume fraction other than the fiber part, or $1 - V_f$. Figure 6 shows the V_f of each sample and also the post-MI bulk densities of only the matrix part obtained from said mercury intrusion porosimetry test, outer dimensions, and weights. The bulk densities in the mercury intrusion porosimetry test were calculated assuming that there is no mercury intrusion into pores at the lowest pressure (approximately 0.035 atm) and by using the bulk volume

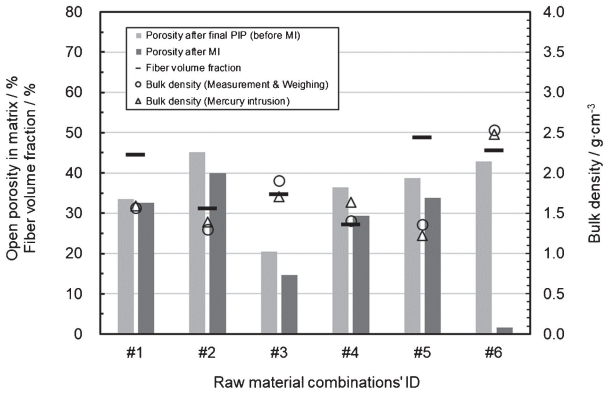

Fig. 6. Open porosities of the matrices in the samples after the last PIP processing and MI processing obtained using the mercury intrusion porosimetry test, as well as the fiber volume fractions and the post-MI bulk densities of each matrix.

of the samples obtained at that time. While the magnitude relationship among the samples of V_f was generated by press forming, it depended significantly on the blending ratio of the solid components in the slurries shown in Fig. 3. The values obtained by both density measurement methods were close to each other in all the samples, supporting the validity of the values obtained by the mercury intrusion porosimetry test.

The open porosity after the last PIP processing was in the range of 30-odd to 45 % for the combinations other than #3. The above-mentioned Document 11 showed a result indicating that it is desirable for the vacancy rate of the green matrix before the MI processing to be around 35 vol %, and the combinations other than #3, but including #1, #4, and #5, are said to be in a state close to this requirement. The magnitude of the open porosity in the PIP processing may be changed to a certain extent depending on the number of times processing is conducted, and it is impacted by the press forming. Therefore, we do not currently have discussions linked to the dense/uniform matrix formation, which is the purpose of this study, and it will be explained in the paragraph after the next, as the basic technology guidelines of PIP processing. First, we will state the results of the MI processing.

While the open porosity by the MI processing lowered by approximately 5 % for most of the samples, the ratio increased by no less than 40 % for #6, and on the contrary, the ratio was as small as several percentage points for #1. These results coincided well with the measurement results by the Archimedes method conducted on the same samples, supporting the validity. As such, it was suggested that the impregnating ability of molten Si was low for the formed microstructures by the existing PIP processing only from SiC materials, and that the C-formed microstructures formed from C precursor polymers was well impregnated by molten Si, of which the specific surface area was raised, and that the microstructures might be highly densified.

The factors impacting the open porosity after the last PIP processing are considered to be the blending ratio of the solid components in the slurries shown in Fig. 3 and the volumetric yields of the slurries shown in Fig. 4. Seeing the results obtained here, the open porosities of #4 and #5 were high, next to #2 and #6 of which the volumetric yields of slurries were low. As a whole, the open porosities depended on the volumetric yields of the slurries. By comparing #1 and #3, we found that the open porosity of #3 was significantly lower than that of #1 in spite of the closeness of their volumetric yields, and, in relation to the above, we surmise that the reason is that the fluidity after the removal of solvents from the slurry of #3 containing fine powders was lower than that of #1, and that the outflow during press forming and thermal processing was kept low. In any case, the impact related to the densification through MI processing due to the open porosity after the last PIP processing was not dominant, at least for the samples targeted in this study, if considering that even the open porosity of #3 lowered similarly to the others in MI processing, and that the open porosity of #1, which had the smallest reduction of open porosity in MI processing, lowered moderately after PIP processing. Therefore, the impact of the combinations of raw materials is considered to be evaluable.

Figure 7 shows the pore size distribution of the matrices only in the samples after the first, second, and last PIP processing and MI processing, obtained by using the mercury intrusion porosimetry test for the respective combinations of raw materials. The diagram for #2 shows the results of the second and later PIP processing, because stable samples sufficient to be provided for the evaluation were not obtained for the first PIP processing. Also, the results lacked around 6 μm for all the diagrams, which showed that the non-continuous lowering behavior was caused by the operation of equipment at this timing, so this part was omitted.

The pore size obtained here is said to be equivalent to the representative diameter of the cross section for almost spherical or cylindrical voids, and to the twice the aperture width of the crack for the crack-like voids, based on the principle of impregnation of mercury into the cylindrical voids.[18] Roughly speaking, the relationship between the pore size and the microstructures of the materials at the early stage of the process, in consideration of the fiber diameter and the fiber reinforcing structure, is considered as follows: the pores of several tens of μm or larger are considered to be large voids among the fiber bundles such as mesh (crossing of fiber bundles) and between the sheets; the pores from several μm to several tens of μm are considered to be relatively small voids that are distributed among and in the fiber bundles; and the pores smaller than several μm are considered to be micro-pores formed due to the raw materials.[19] As the processes advance, the voids impregnated with raw materials diminish in size, and the voids that closed as a result of the diminishment of their own diameter or a route from the outside become closed pores.[20]

The characteristic common to all the diagrams clarified that #1 and #2, #3 and #4, and #5 and #6 in the same raw material types showed close aspects respectively. In #1 and #2, the aspects differed in the range of up to several tens of μm for the early stage of PIP, but became close in the entire range after the last PIP processing, and the pore size showed a similar distribution from one-digit μm to the second half of two-digit μm, with its peak at around several tens of μm after MI processing. The pore sizes in the range of up to several tens of μm in the early stage of PIP processing of #1, in consideration of the difference in raw material composition from that of #2, are guessed to be distributed in the microstructures formed by thermal decomposition caused by SiC powder. For both #3 and #4, the pore size distribution was constantly flat from one-digit μm to the first half of two-digit μm in the early stage of PIP processing, but as the processes advanced, the pore size in the range of mainly one-digit μm decreased. There was no significant change in the distribution shape before and after MI processing, and the pore size showed a

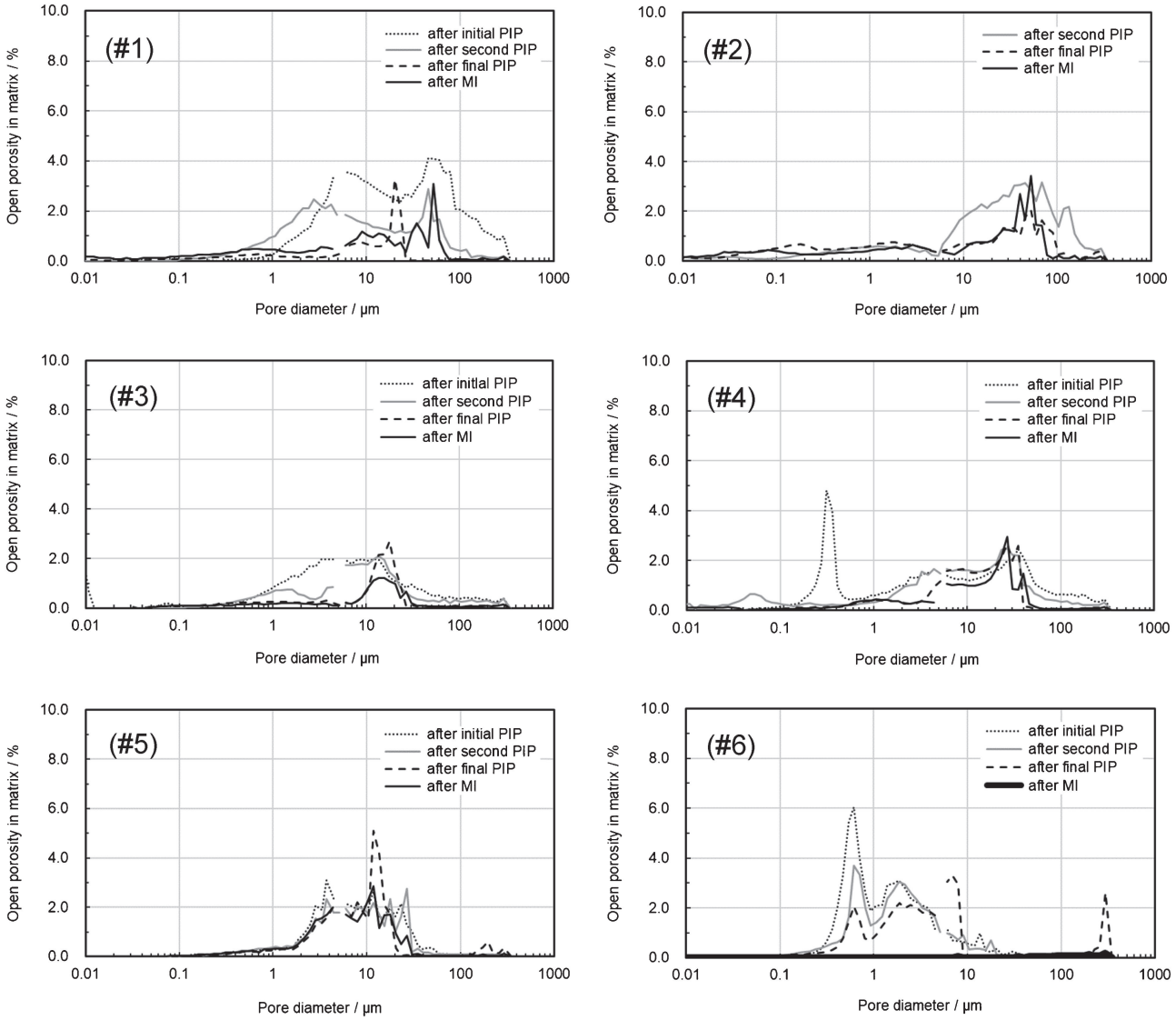

Fig. 7. Pore size distribution diagrams of the matrices in the samples after the first, second and last PIP processing, and MI processing, obtained using the mercury intrusion porosimetry test.

distribution with its peak for slightly smaller diameters than the samples of #1 and #2. For only #4, a sharp peak was recognized for sub-μm after the first PIP processing, and it disappeared in the second processing. In consideration of the difference in raw material composition from that of #3, this is deemed to have been clearly caused by the pore-forming powder. Samples #1 to #4, which were based on the same precursor polymer, showed pore distribution commensurate to the respective raw materials in the first PIP processing, but all of them showed of behavior enhancing densification in subsequent processing, except for in the range of several tens of μm. Samples #5 and #6 were based on different precursor polymers, so their aspects were significantly different from those of the above. They showed a distribution centering on one-digit μm, which was related to the impregnating ability of slurries, but there was little change caused by the repetition of PIP processing. Sample #6 showed a peak of sub-μm, similarly to #4, and the peak was detected also after the last PIP processing. For #5, the pore size showed little change in distribution before and after MI processing, while for #6, it was almost zero in the entire range after MI processing.

The peak of sub-μm caused by the pore-forming powder, which was detected only in #4 and #6, also appeared in #2, in which the pore-forming powder was similarly blended, after the first PIP processing, but the peak was not detected, which we surmise was due to the filling of pores from after the second PIP processing, similarly to the case of #4. While the micropores were no longer detected from the second PIP processing onward for #2 and #4, they continued to be detected even after the last PIP processing for #6, although they decreased as PIP processing was repeated. This may depend on the extent of impregnation of slurries into the micropores, and also on the blending conditions of slurries. Basically, the above is thought to be related to the relatively low viscosity and high wettability of the precursor polymers used for #5 and #6, and to the

smaller pore diameter distribution in the heat decomposed substances formed therefrom.

3.2 Comparison of microstructure/composition distribution among the raw material combinations

Figure 8 shows the conformation and compositional distribution images of the respective raw material combination samples by EPMA. The upper row of the respective samples shows images after the last PIP processing (before MI processing), and the lower row shows images after MI processing. From left to right, they show the compositional image in BSE mode, Si elemental mapping, and C elemental mapping. The color scale corresponding to the respective detection strengths of Si elements and C elements was unified for before and after MI processing and for all the samples. The entire densification level of the samples is discussed based on the measurement results shown in Fig. 6.

In identifying the composition in the images, firstly, as the long and continuous shapes show the fibers that contained Si atoms and C atoms at a proportion close to the stoichiometric composition of 1:1, we determined the amount of respective elements based on comparison with this color. As all the slurries for #1 to #6 contained at least either the SiC precursor polymer or the SiC powder, assuming that the powders in slurries were almost uniformly dispersed, we determined that the areas from which the Si element was not detected before the MI processing at all, in other words, the black areas in the Si elemental mapping, are the voids where the PIP-derived green matrix was not formed. Said areas are shown in red in the C element mapping, and the C element concentration is particularly high, which derives from the epoxy resin that was used in the resin-embedding of said samples. For the areas from which the C element was not detected at all after MI processing, and simultaneously, where the Si element concentration was higher than that of the fiber, we determined that molten Si had impregnated the areas where a PIP-derived green matrix was not formed and remained there, becoming residual Si.

Taking note of the change before and after MI processing in the respective raw material combinations and the differences among them, we discuss the factors based on the foregoing results on the density. Microstructures after the last PIP processing of #1 were formed only in the fiber bundles and their surroundings and showed the aspect commonly seen in the PIP densification process similarly to the below-mentioned sample of #5. It was observed that there seemed to be a space in which the molten Si penetrated into all the samples in MI processing, but as seen on the lower side of the image after MI processing, molten Si remained only around the surface of the samples. We surmise that the flow paths in front became clogged so the molten Si was not able to go further forward in the process of penetration of molten Si associated with the decomposing reaction of the surrounding thermally decomposed SiC microstructures with low crystallizability. It is thought that the foregoing is related to the result that the reduction of porosity of #1 in the MI processing was the lowest, as shown in Fig. 6.

The volumetric yield of slurry of #2 was probably lower than that of #1, so the porosity after the last PIP processing was high and the voids remained among the meshes and between the lamination layers even after MI processing, so the porosity remained high. On the other hand, massive microstructures, which were not observed in #1, were formed between the lamination layers, and it is thought to have been caused by the exertion of the macro volume-reduction restricting effect until the hardening of precursor polymers by the pore-forming powder, similarly to the other fine powders. In MI processing, in contrast to #1, molten Si impregnated the fiber bundles and interlayers of the entirety of the samples to a certain extent, and the voids were filled as shown in the figure. The ratio was similar to that of other samples, except #1. The reason for the increased impregnating ability of molten Si in comparison with #1 is thought to be that the micropores from the pore-forming powders were formed in the entire formed microstructures and that the microstructures were connected in co-existence with the micro-cracks caused by the heat-decomposing shrinkage of precursor polymers, causing the infiltration paths of molten Si to increase on a micro level, and blocking became difficult. The formed microstructures that came into contact with molten Si were fragmented.

For #3, the PIP-derived microstructures were formed relatively densely in accordance with the results of Fig. 6. We surmise that the outflow of slurries was controlled due to the dispersion of C particles, which also had smaller particle diameters in comparison with #1, to which the raw material structure was the closest. In spite of the smaller space into which molten Si may impregnate compared with other samples, the aspect of molten Si penetrating into the entirety of the samples was observed in the Si element mapping after MI processing. Nevertheless, there were parts that were shown in blue in the Si element mapping and in green to red in the C element mapping, which are deemed to be the phase where the C powder contained in the PIP-derived microstructures remained without reacting with molten Si, and in contrast to the foregoing two samples, the phase had a non-uniform property, including the C-rich phase.

For #4, PIP-derived microstructures were formed in a large mass between the lamination layers more extensively than those of #3. The microstructures were clearly separated by the vertical cracks made at intervals of approximately 200 μm on the lamination plane, and it is thought that the microstructures were thermally decomposed and reduced after hardening-formation under the high shape retaining property of the pore-forming powders. In MI processing, molten Si was widespread to a certain extent, similarly to #2, by the large cracks and the micropores from the pore-forming powder. Also, similarly to #2, the formed microstructures that came into contact with molten Si were fragmented.

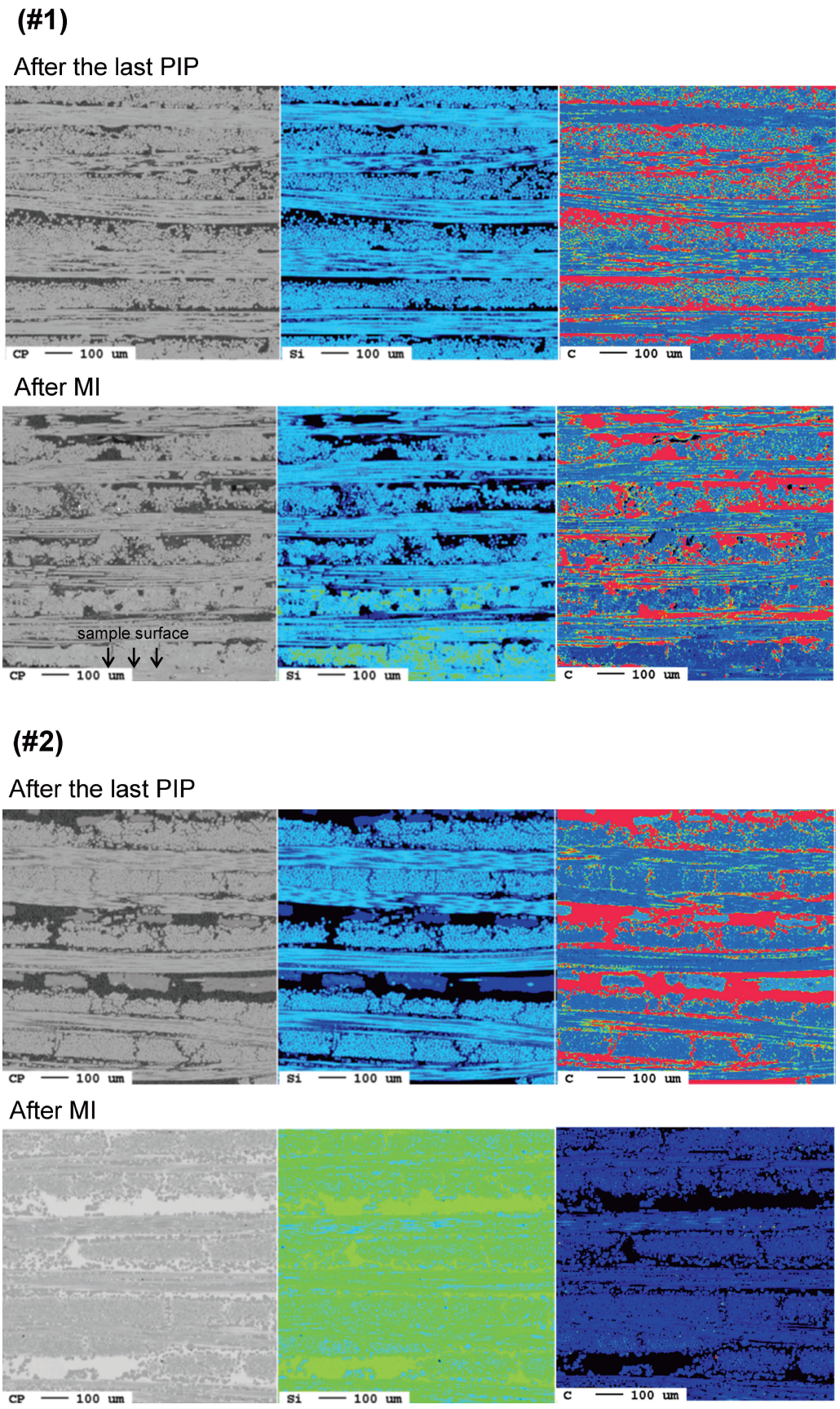

Fig. 8. *Continued on next page.*

(#3)

After the last PIP

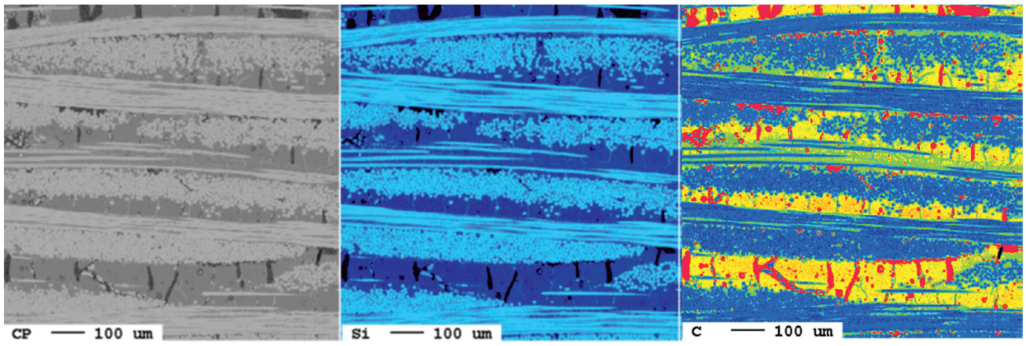

After MI

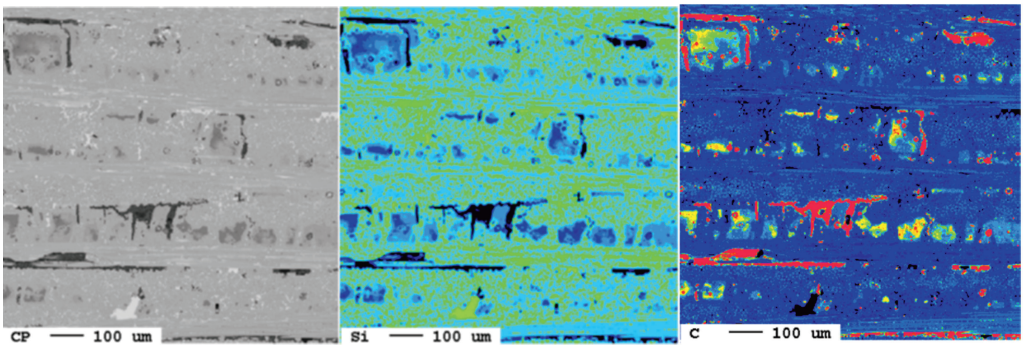

(#4)

After the last PIP

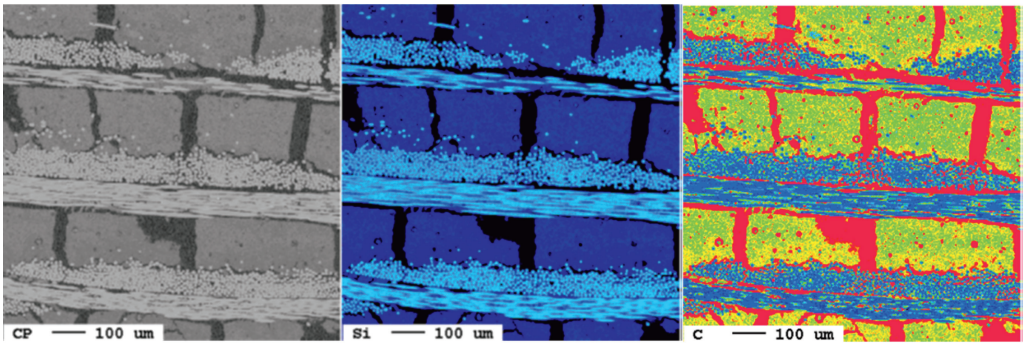

After MI

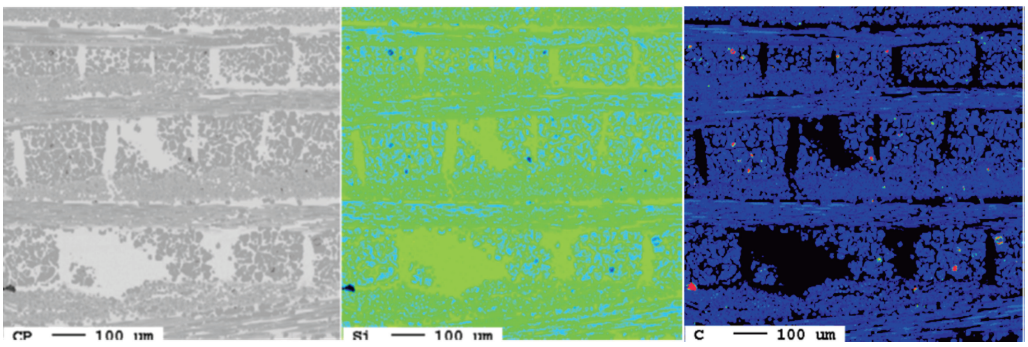

Fig. 8. *Continued on next page.*

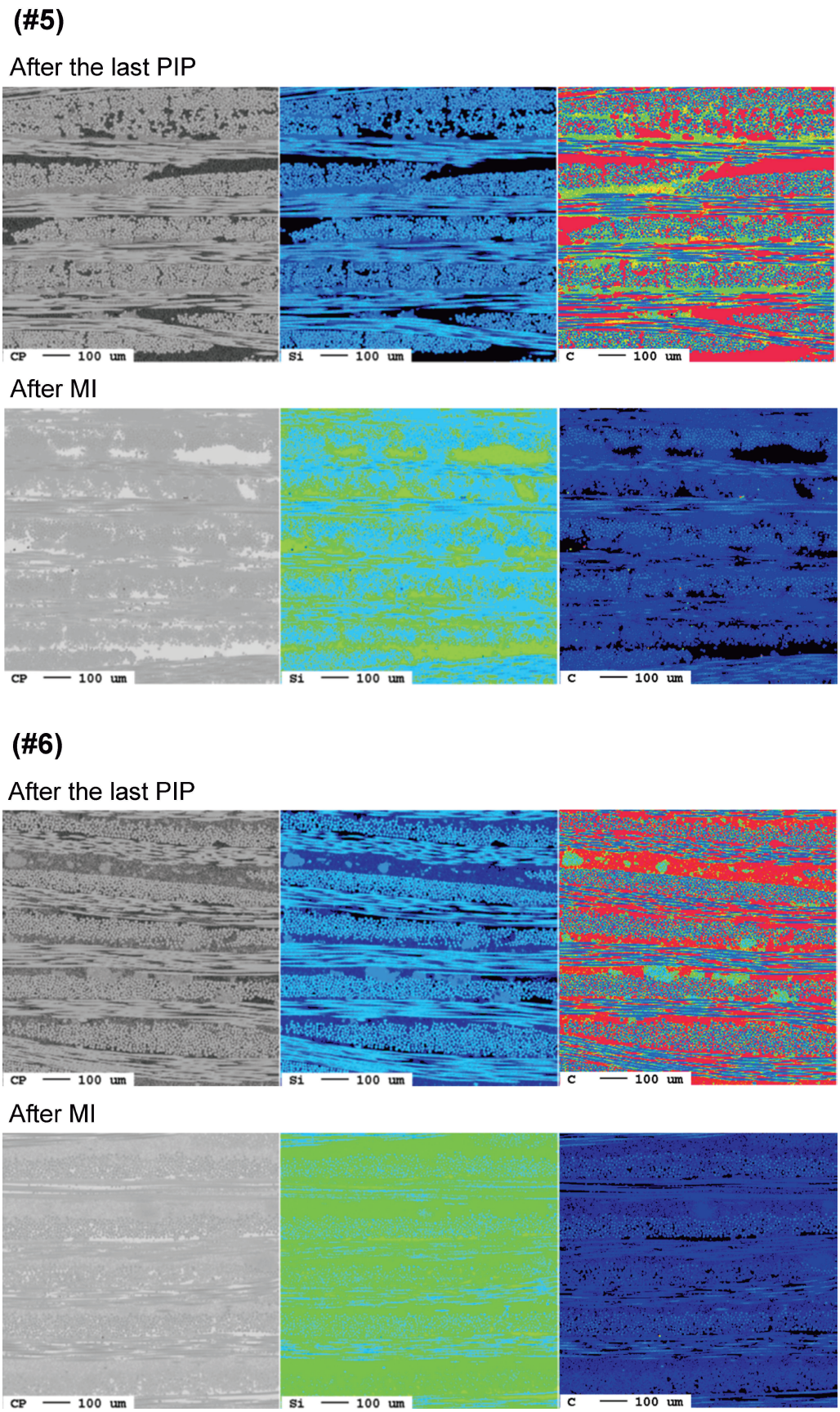

Fig. 8. EPMA results of the samples #1–#6 after the last PIP processing (upper) and MI processing (lower). Compositional image in BSE mode (left), and elemental mappings of silicon (center) and carbon (right).

For #5, microstructures were formed only in the fiber bundles and their surroundings, similarly to #1 after the last PIP processing. After MI processing, however, in contrast to #1, the molten Si impregnated well to a certain extent. Similarly to #3, the fragmentation of PIP-derived microstructures seen in #2 and #4 was, at least, not notably observed.

For #6, PIP-derived microstructures were generally formed quite uniformly compared with the others, and the molten Si impregnated all over from the MI processing. It cannot be said that #6 is advantageous in the formation of uniform microstructures compared to the others both in the ratio of solid components in slurries and the volumetric yield after thermal processing. In PIP processing, considering the correlations between the other raw material compositions and the generated microstructures, we surmise, in addition to the enhancement of continuity of the microstructures during hardening formation by the pore-forming powder as in #2 and #4, that local volume shrinkage occurred in the entire area in relation to the low thermal decomposing yield of precursor polymers, and that the tendency of cracks to occur at a specific area as in #4 was low, which might have contributed to the formation of uniform microstructures. In MI processing, molten Si impregnated the entirety of the samples by micropores caused by pore-forming powder, and furthermore, as shown in Fig. 7, most voids were as small as 10 μm or less. The reaction density with molten Si was high, and the outflow was restricted with the power of capillary force, from which it is thought that almost all the voids were filled.

From the foregoing, we will discuss some results with a view to #1 to #6. Concerning the insufficient infiltration of molten Si in only #1, considering that Sample #3, which was denser based on the same precursor polymer, was densified at the same level as the other samples, it cannot be said that the insufficient infiltration was caused by the lack of voids into which molten Si would infiltrate. The largest difference between #1 and #3 was the presence or absence of C components in the PIP green matrix. On the other hand, the same level of densification as the other samples occurred in #2 which did not contain the C component. Despite this, the voids to be the paths of molten Si in #2 existed in a higher density than #1 due to the distribution of micropores. In view of this, favorable Si impregnation was not obtained in the MI processing on the green matrix obtained under the existing PIP conditions, but it is thought that the above situation was improved by the distribution of voids at a higher density in the green matrix, or by having the C component contained within a certain range of conditions. The main factor of promotion of impregnation by having the C component contained is foreseen to be the improvement of the driving power of impregnation by the existence of C, which is the target of the reaction, in front of the impregnation of molten Si, but a separate investigation is required for clarification.

We will now discuss the fragmentation of PIP-derived microstructures after the MI processing on Samples #2 and #4. As shown in Fig. 7, most micropores formed in the first PIP processing on these samples became clogged or were isolated from the outside in the second processing. As the representative aspect thereof, **Fig. 9**(a) shows a photo from a metallurgical microscope observation on the polished plane after the last PIP processing of #4. The inhibition of impregnation of molten Si due to clogging/insolation was a concern, but relatively favorable impregnation was confirmed from Fig. 8, and it is surmised that the non-continuous form of the former distribution of micropores had an effect on the impregnation of molten Si. After MI processing, the original microstructures were fragmented as shown in Fig. 9(b), which was significantly different from Fig. 9(a). It is surmised that the phenomenon was caused by the polymer thermal-decomposition-formed SiC, which was common to #2 and #4, and occurred in accordance with the micro volume change and the direction of crystallization at the time of the decomposition reaction due to the encounter of SiC of low crystallizability with molten Si. A separate investigation is also required for detailed clarification of this phenomenon.

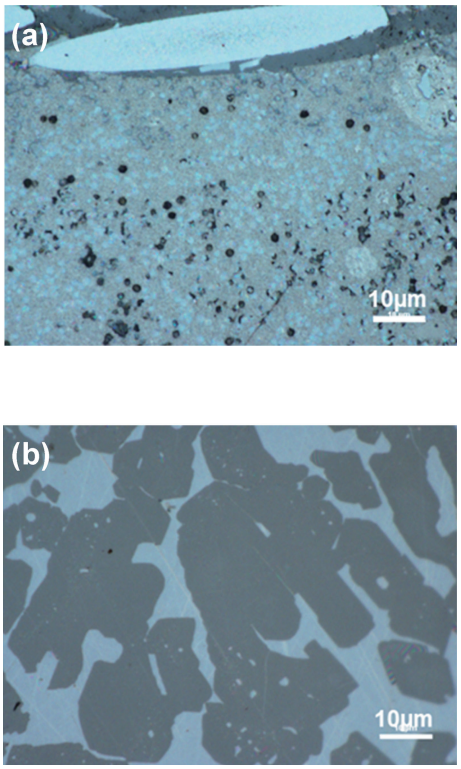

Fig. 9. Metallurgical microscope images of the polished surfaces of the #4 sample: (a) after the last PIP processing, and (b) after MI processing.

Now we will discuss the MI-formed micro microstructures and the composition of #6. As shown in Fig. 8, uniform microstructures with fewer defects from pre-MI to post-MI processing, and with the distribution of both Si elements and C elements in the entire image were formed on this sample. Nevertheless, if comparing the colors of the formed microstructures in the distribution image of Si elements after MI processing and the SiC fibers that almost represented stoichiometric composition, it is suggested that

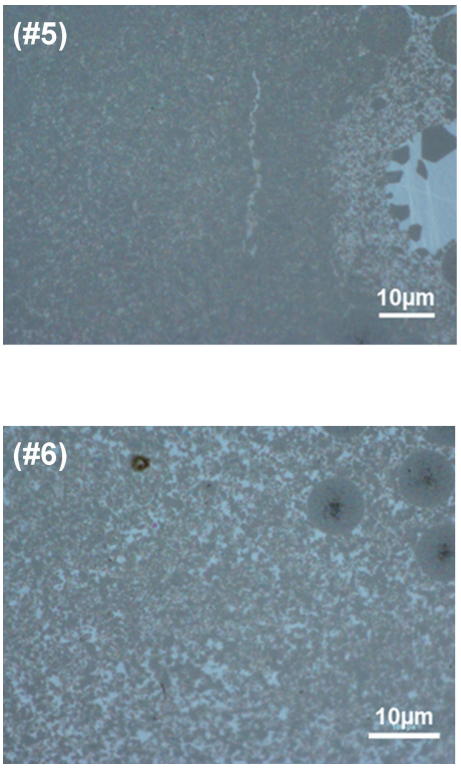

Fig. 10. Metallurgical microscope images of the polished surfaces of the samples #5 and #6 after MI processing.

the microstructures were richer in Si. On the other hand, if #5 is compared in the same way, the image is observed to be closer to the stoichiometric composition. In the highly magnified photo with the metallurgical microscope of #6 shown in **Fig. 10**, the Si phase of no greater than several μm looks relatively bright, and is distributed all over, which corresponds exactly to the distribution of pore diameter shown in Fig. 7. The Si phase that was finely distributed is considered to be the main reason for the Si-rich appearance in Fig. 8. In Fig. 10 (#5), such Si phases were limited to only around the surface of green matrix that came into contact with the molten Si as shown in the right side of the photo.

3.3 Comparison of thermal and mechanical properties among the raw material combinations

Figure 11 shows the measurement results of the thermal conductivities of composite samples after the MI processing of respective raw material combinations. Figure 11(a) shows the values from the ambient temperature to high temperature of the entirety of the materials. While all the samples showed representative behaviors of SiC that decreased in line with the temperature rise, only the values of Sample #6, in particular, shifted at a high level equivalent to that of high-purity SiC all over the temperature areas, and recorded 65 $W \cdot m^{-1} \cdot K^{-1}$ at ambient temperature and 25 $W \cdot m^{-1} \cdot K^{-1}$ at 1200 °C. As explained above, this is because it was possible to form a dense and uniform matrix with few pores through the collaboration of PIP and

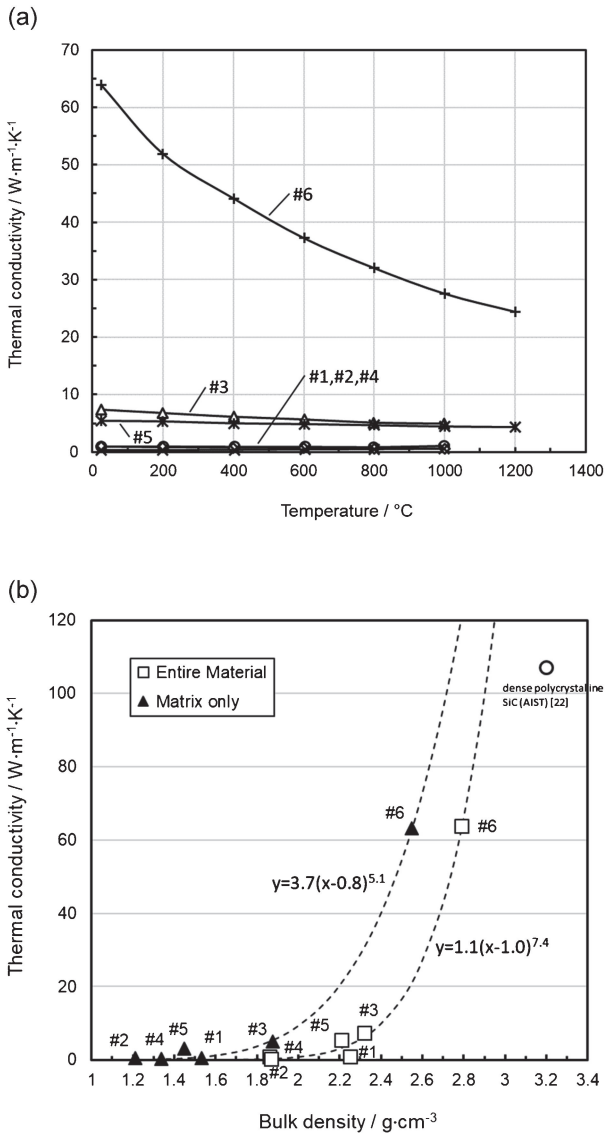

Fig. 11. Thermal conductivities of the composite specimens perpendicularly to lamination plane: (a) dependency on temperature for the entire material, (b) dependency of thermal conductivity at 25 °C on the bulk densities of the entire material and the matrix only.

MI processing. The values of the other five samples did not reach 10 $W \cdot m^{-1} \cdot K^{-1}$ even at ambient temperature, and they attained a level that has often been reported for SiC/SiC composites formed by the PIP method.[21] As shown in the pore distribution and the results of microstructure observation, these samples were microstructures of low continuity that have taken over the PIP-derived microstructures. Furthermore, if a highly crystalline SiC layer is formed on fibers, or what is more, on fiber bundles, with the CVI processing that has been performed as standard in recent years, the layers largely contribute to improving the thermal conductivity of the materials, which require caution in the evaluation of material data.

Figure 11(b) shows the plotting of the relationship between thermal conductivity and bulk density at 25 °C only for the entirety of the materials and the matrices. We

added the literature data of high-density polycrystalline SiC to the same figure for reference.[22] In all of these, there is a visible trend for the thermal conductivity to increase at an accelerated pace together with the increase of bulk density, and #6 showed a higher value largely different from the others in terms of both bulk density and thermal conductivity. Thermal conductivity, together with specific heat and thermal diffusivity, was multiplied linearly with the bulk density; herein, bulk density is related to the degree of porosity, and changes in porosity have an impact on the specific heat and thermal diffusivity. These have appeared comprehensively in thermal conductivity. The impact of porosity on the thermal conductivity of porous ceramics is examined based on the heat transfer formula and the compound rule, but no versatile theoretical formula has been established.[23] The function shown in the figure was obtained by placing an approximation curve as a power function and using the solver function of Microsoft® Excel® for Office 365. This empirical formula can be used as an effective standard for the thermal conductivity of SiC/SiC composites based on PIP and MI.

Figure 12 shows the results of Young's modulus measured by the resonance method from the ambient temperature to 1400 °C for the unidirectional reinforced composite samples of respective raw material combinations. Figure 12(a) shows the change of Young's modulus of the entirety of the materials by temperature. The values at ambient temperature vary across a wide range of 150 GPa to over 300 GPa, there was no large change by temperature in any of the samples, and their relative relationship was mostly kept to a high temperature. Young's modulus decreased little by little in line with the temperature rise of most of the samples, and the decreasing gradient became larger from around 1400 °C. We surmise that the behavior in the latter half is caused by the softening of the residual Si due to high temperature, which is one of the challenges of MI processing. It was found that this impact became conspicuous from the latter half of the 1300 °C range. Furthermore, Samples #1 and #3 showed little decrease in elastic modulus caused by the temperature rise, when compared with #2, which changed on the same level. The common characteristics were that they were based on SiC precursor polymers, and that molten Si did not spread all over.

Figure 12(b) shows the plotting of bulk density for the entirety of the materials and the matrix only, and Young's modulus at 25 °C. In both of them, Young's modulus increased in line with the increase of bulk density with a certain extent of the relationship, and the uniformity of plotting on the entirety of the materials was high in particular. In a document that applied the percolation theory to forecast the elastic modulus of porous ceramics materials,[24] it was reported that the elastic modulus follows the power function, such as 2.1 power of the density. Based on this theory, we sought an approximate curve of plotting for the entirety of the materials in the form of a power function using the solver function of Microsoft® Excel® for Office 365, and obtained the power function of the bulk density

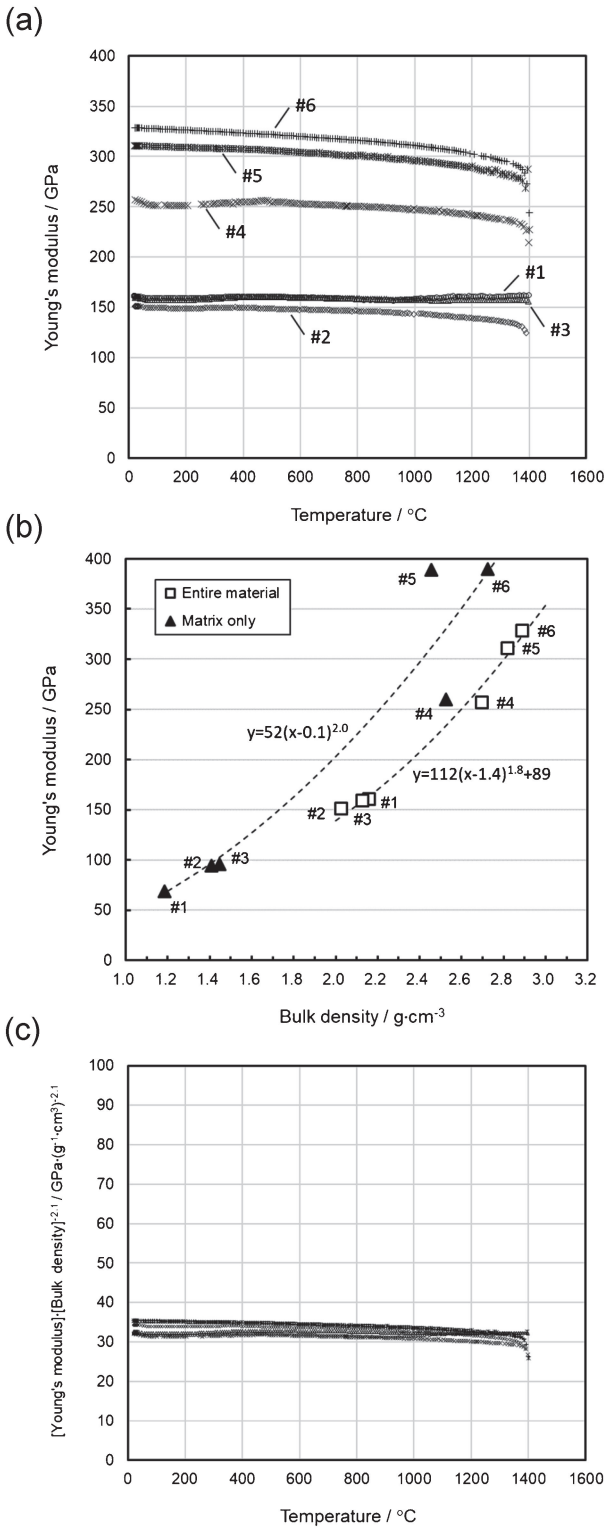

Fig. 12. Impulse excitation test results of the unidirectional composite specimens longitudinally to fiber orientation: (a) Young's moduli as a function of temperature, (b) dependency of Young's moduli at 25 °C on the bulk densities of the entire material and on the matrix only, and (c) dependency of percolation model-based calculated values on temperature.

to the power of 1.8. We conducted a similar investigation for the matrices only, and obtained the power function of the bulk density to the power of 2.0. In the above-

mentioned document, the X intercept is deemed to be the threshold of the density from which the material starts to present its elastic modulus. For the matrices only, a behavior in accordance with this was recognized, in other words, a behavior where the matrix elastic modulus starts to rise from 0.1 $g \cdot cm^{-3}$ according to the curve established herein. Taking note of the constant of the power function from a similar viewpoint on the entirety of the materials, a behavior was observed where the appearance of 89 GPa starts from the bulk density of 1.4 $g \cdot cm^{-3}$. Here is an estimate: if uni-directionally aligned fibers are solidified up to a barely unified state in which $V_f = 40\,\%$ and the matrices are filled to approximately 10 % of the other space, or a state in which $V_f = 30\,\%$ and the matrices are filled to approximately 30 % of the other space, said elastic modulus starts to appear, leading to a situation in which the elastic modulus increases at an accelerated pace in accordance with the space filled by any of the elements. As a calculation based on this relationship, the Young's modulus of the entire material divided by 2.1 power of its bulk density clarified the data that overlapped well in the whole temperature ranges for all the samples as shown in Fig. 12(c). The data did not overlap like this in the cases of the 2.0 or 2.2 power. A separate detailed investigation is required for the physical interpretation of the above.

As seen above, we investigated the densities, pore diameter distributions, and composition distribution depending on the raw material combinations on the SiC/SiC composites based on PIP-MI, and we discovered that both their thermal conductivity and elastic modulus strongly depended mainly on the bulk density, among different factors.

3.4 Outlook for improvement of microstructures depending on the blending ratios in the respective raw material combinations

The comparative evaluations among the raw material combinations described so far were conducted by selecting the blending ratios that are deemed to be suitable for each one, based on the concept explained in Section 2.2. Based on the results obtained therein, we discussed the improvement of microstructures by adjusting the blending ratios in the raw material combinations and verified the discussion by conducting experiments in part.

For Samples #1, #3, and #5 in which pore-forming powder is not blended, large voids can be diminished in size and the PIP-derived microstructures may be somewhat uniformized by increasing the blending ratios of SiC/C powders in consideration of the impregnating ability. However, there have been challenges, namely the difficulty of impregnation of molten Si for #1, and unreacted residue from a part of C-containing microstructures for #3, so it is difficult to increase the blending ratio of powders in the process using the MI processing. On the other hand, as there was no conspicuous occurrence of insufficient impregnation of molten Si or unreacted residue of formed microstructures, it is expected that these microstructures will be improved to a certain extent by increasing the powder blending ratio within the permissible scope, including the impregnating ability of slurries. In the studies on C/C-SiC composites,[25] unreacted residue of green matrices derived from phenol resin was commonly seen after the impregnation of molten Si. It is surmised that the favorable impregnation of molten Si into the C precursor polymer-formed microstructures in this study was caused by the thermal decomposing yield ($\approx 30\,wt\,\%$) of the subject polymer, which was not high, and by the formation of micropores that were distributed as shown in Fig. 7 (#5), in the thermal decomposition products of the slurries in which the subject polymer and SiC powder were blended. A separate investigation is required to clarify the details.

Among the samples #2, #4, and #6 in which pore-forming powder was blended, large voids were formed between the lamination layers of PIP-based microstructures of #2, and large cracks were formed in the longitudinal direction between the lamination layers of the microstructures of #4, both of which led to non-uniform microstructures after the MI processing. These were mainly caused by the thermal decomposing shrinkage of slurries, so, to mitigate the apparent shrinkage, we verified the improvement effect of non-uniform characteristics of the microstructures through experiments, by blending SiC powder, or increasing the blending ratio thereof.

For Sample #2, with the blending ratio in the raw materials excluding the solvent shown in Fig. 3(b), we prepared and evaluated the samples in which 10-odd vol % of pore-forming powder of #2 was replaced with SiC powder. The blending ratio of SiC powder shown in said figure was herewith almost similar to that of #1, and the volumetric yield from the raw materials excluding the solvent shown in Fig. 4(b) was considered to be equal to that of #4 and #6. The sample prepared under these conditions was called "#2*". **Figure 13** shows a microscope photo of the polished cross section of the representing microstructures and a photo of #2. In #2*, there is a whitish look to the areas that are not well polished due to the fragility of the thermal decomposition-formed microstructures, including the micropores, and a dark look to the parts that are relatively well polished into a plane. As the volumetric yield of the slurries was enhanced, the PIP-derived microstructures between the lamination layers increased, compared with #2, but it seems that molten Si did not infiltrate inside since the crack-like voids remained and the paths for impregnation became narrow. Although #2* can be seen as a sample with micropores formed by replacing some of the #1 precursor polymer with pore-forming powder, the impregnation of molten Si was not improved from #1.

For Sample #4, we prepared the sample by increasing the C powder and pore-forming powder of Fig. 3(b) #4 to approximately 1.3 times their blending ratio without changing the relative ratio and then evaluated the sample. In doing this, we intended to reduce the longitudinal cracks in the lamination plane caused in #4 by improving the volumetric yield after thermal processing and the shape-retaining property with the pore-forming powder. We call the sample "#4*". **Figure 14** shows a microscope photo of the polished cross section of #4* and a photo of #4. In #4*,

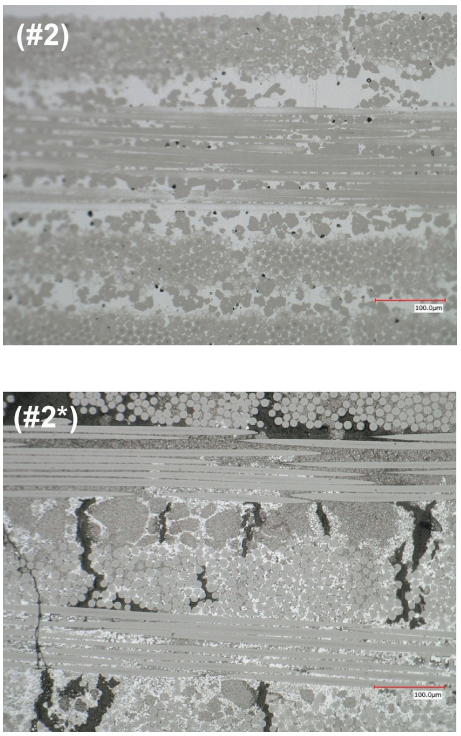

Fig. 13. Microscope images of the polished surfaces of the samples #2 and #2* after MI processing. #2* was made with slurry in which more than 12 vol.% of pore-forming powder of #2 was replaced with SiC powder.

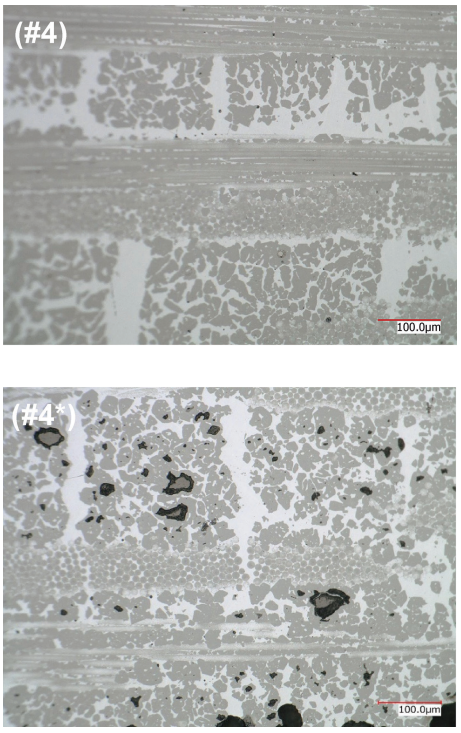

Fig. 14. Microscope images of the polished surfaces of the samples #4 and #4* after MI processing. #4* was made with a slurry in which the blending ratio of C powder and pore-forming powder was increased by around 1.3.

there was hardly any inhibition of longitudinal crack formation; rather, there was an increase in the voids that are thought to be caused by the decrease of fluidity of slurries.

From the above discussions together with the implemented examples, although it is very limited, it is thought that there is little room for improvement of microstructures by adjusting blending ratios in the raw material combinations, and the effect is smaller than in the case of selection of raw material combinations. We believe that effective approaches are to narrow down the combinations to the blending of C precursor polymers and fine powders such as SiC and pore-forming material, and to elaborate the specifications and blending conditions of the respective raw materials.

4. Conclusion

Aiming for the acquisition of dense and uniform SiC matrices from raw materials containing precursor polymers through PIP-MI processing, we investigated the combinations of suitable raw materials and their blending ratios. The results obtained are listed below:

(1) Among the combinations of precursor polymers that form SiC and the powder, the combination of C precursor polymers added with SiC powder and pore-forming powder was the most effective in terms of both densification and uniformity.

(2) Both the thermal conductivity and the elastic modulus depended on the density of the materials most strongly, and improved at an accelerated pace in line with the increase in density.

(3) Molten Si has a poor impregnating ability with regard to the SiC microstructures under the existing PIP conditions. It was suggested, however, that the impregnating ability can improve to a certain extent by forming porous structures to increase the paths and by containing C, which would be the reaction partner.

(4) Porous microstructure formation by blending pore-forming powder was effective as it did not leave unreacted green matrices after MI processing. It was found, however, that fragmentation of microstructures would occur if having molten Si impregnate into the continuous porous microstructures formed from the SiC precursor polymer.

Acknowledgments These outcomes were obtained as the result of a commission project of the New Energy and Industrial Technology Development Organization (NEDO) (JPNP15006). We would like to express our appreciation to Dr. Masahiro Hojo, Dr. Takeshi Yamamoto, and Dr. Shigeru Tachibana (Aeronautical Technology Directorate, Japan Aerospace Exploration Agency (JAXA)), who provided all kinds of technical cooperation for the achievement of this study. We also express our appreciation for Ms. Emi Goto (Human Resocia Co., Ltd.) and Ms. Wakana Sekiguchi (Adecco Co., Ltd.) for their cooperation in some experiment operations.

References

1) J. Steibel, *Am. Ceram. Soc. Bull.*, **98**, 30–33 (2019).
2) A. R. Bunsell and A. Piant, *J. Mater. Sci.*, **41**, 823–839

(2006).
3) R. R. Naslain, R. J. F. Pailler and J. L. Lamon, *Int. J. Appl. Ceram. Tec.*, 7, 263–275 (2010).
4) J. A. DiCarlo, H.-M. Yun, G. N. Morscher and R. T. Bhatt, in "SiC/SiC Composites for 1200 °C and Above", Ed. by N. P. Bansal, Springer, Boston (2005) pp. 77–98.
5) A. Lacombe, P. Spriet, A. Allaria, E. Bouillon and G. Habarou, 50th AIAA/ASME/ASCE/AHS/ASC Structures, Structural Dynamics, and Materials Conference, May 4–7, Palm Spring, America (2009) AIAA 2009-2675.
6) M. B. Ruggles-Wrenn, N. J. Boucher and C. P. Przybyla, Proceedings of the ASME Turbo Expo 2018: Turbomachinery Technical Conference and Exposition, June 11–15, Oslo, Norway (2018) V006T02A001.
7) S. Denneulin, 10th International Conference on High Temperature Ceramic Matrix Composites, Sept. 22–26, Bordeaux, France (2019) 1970.
8) J. Lamon, in "Chemical Vapor Infiltrated SiC/SiC Composites (CVI SiC/SiC)", Ed. by N. P. Bansal, Springer, Boston (2005) pp. 55–76.
9) S. Zhao, Z. Yang, X. G. Zhou, X. Z. Ling, L. S. Mora, D. Khoshkhou and J. Marrow, *Tech Science Press*, 42, 103–124 (2014).
10) Y. Gowayed, G. Ojard, R. Miller, U. Santhosh, J. Ahmad and R. John, April (2007) AFRL-ML-WP-TP-2007-472.
11) S. Suyama, Y. Itoh, A. Kohyama and Y. Katoh, *J. Ceram. Soc. Jpn.*, 109, 315–321 (2001) [in Japanese].
12) S. Suyama, T. Kameda and Y. Itoh, *J. Ceram. Soc. Jpn.*, 109, 619–626 (2001) [in Japanese].
13) M. Sato, M. Suzuki, Y. Tanaka, Y. Inoue, N. Miyamoto, T. Ishikawa, Y. Katoh and A. Kohyama, 26th Annual Conference on Composites, Advanced Ceramics, Materials, and Structures: A: Ceramic Engineering and Science Proceedings, Volume 23, Ceramic Engineering and Science Proceedings, Jan. 13–18, Cocoa Beach, America (2002) pp. 519–526.
14) B. Mainzer, K. Roder, L. Wöckel, M. Frieß, D. Koch, D. Nestler, D. Wett, H. Podlesak, G. Wagner, T. Ebert and S. Spange, *J. Eur. Ceram. Soc.*, 36, 1571–1580 (2016).
15) M. Kotani, Y. Katoh, A. Kohyama and M. Narisawa, *J. Ceram. Soc. Jpn.*, 111, 300–307 (2003).
16) M. Kotani, K. Nishiyabu, S. Matsuzaki and S. Tanaka, *J. Ceram. Soc. Jpn.*, 119, 563–569 (2011).
17) Ube Industries, ltd., "Tyranno Fiber®" (https://www.ube.com/contents/en/chemical/continuous_inorganic_fiber/tyranno_fiber.html), August 2020.
18) M. Takahashi and W. Lin, *Shigen-to-Sozai*, 120, 455–460 (2004) [in Japanese].
19) S. Suyama, T. Kameda and Y. Itoh, *J. Ceram. Soc. Jpn.*, 108, 854–860 (2000) [in Japanese].
20) M. Kotani, T. Inoue, A. Kohyama, K. Okamura and Y. Katoh, *Compos. Sci. Technol.*, 62, 2179–2188 (2002).
21) R. Yamada, T. Taguchi, J. Nakano and N. Igawa, 23rd Annual Conference on Composites, Advanced Ceramics, Materials, and Structures: A: Ceramic Engineering and Science Proceedings, Volume 20, Ceramic Engineering and Science Proceedings, Jan. 25–29, Cocoa Beach, America (1999) pp. 273–280.
22) National Institute of Advanced Industrial Science and Technology (AIST), "Thermophysical Properties Database System" (https://tpds.db.aist.go.jp/tpds-web/index.aspx), August 2020.
23) For example: D. S. Smith, A. Alzina, J. Bourret, B. Nait-Ali, F. Pennec, N. Tessier-Doyen, K. Otsu, H. Matsubara, P. Elser and U. T. Gonzenbach, *J. Mater. Res.*, 28, 2260–2272 (2013).
24) J. Kováčik, *J. Mater. Sci. Lett.*, 18, 1007–1010 (1999).
25) M. Patel, K. Saurabh, V. V. B. Prasad and J. Subrahmanyam, *Bull. Mater. Sci.*, 35, 63–73 (2012).